Phase I Technical Report.

Phase I Grant Award Number: DE-SC0013117
Sponsoring Program Office: Office of Science

Recipient Company: Electron Optica, Inc.

Title: PULSE COMPRESSOR WITH ABERRATION CORRECTION

Principal Investigator: Marian Mankos

Topic: 7 - Instrumentation for Electron Microscopy and Scanning Probe Microscopy

Subtopic: a - Electron Microscopy and Spectroscopy

Summary.

In this SBIR project, Electron Optica, Inc. (EOI) is developing an electron mirror-based pulse compressor attachment to new and retrofitted dynamic transmission electron microscopes (DTEMs) and ultrafast electron diffraction (UED) cameras for improving the temporal resolution of these instruments from the characteristic range of a few picoseconds to a few nanoseconds and beyond, into the sub-100 femtosecond range. The improvement will enable electron microscopes and diffraction cameras to better resolve the dynamics of reactions in the areas of solid state physics, chemistry, and biology.

EOI's pulse compressor technology utilizes the combination of electron mirror optics and a magnetic beam separator to compress the electron pulse. The design exploits the symmetry inherent in reversing the electron trajectory in the mirror in order to compress the temporally broadened beam. This system also simultaneously corrects the chromatic and spherical aberration of the objective lens for improved spatial resolution. This correction will be found valuable as the source size is reduced with laser-triggered point source emitters. With such emitters, it might be possible to significantly reduce the illuminated area and carry out ultrafast diffraction experiments from small regions of the sample, e.g. from individual grains or nanoparticles.

During phase I, EOI drafted a set of candidate pulse compressor architectures and evaluated the trade-offs between temporal resolution and electron bunch size to achieve the optimum design for two particular applications with market potential: increasing the temporal and spatial resolution of UEDs, and increasing the temporal and spatial resolution of DTEMs.

Specialized software packages that have been developed by MEBS, Ltd. were used to calculate the electron optical properties of the key pulse compressor components: namely, the magnetic prism, the electron mirror, and the electron lenses. In the final step, these results were folded into a model describing the key electron-optical parameters of the complete pulse compressor. The simulations reveal that the mirror pulse compressor can reduce the temporal spread of UEDs and DTEMs to the sub-100 femtosecond level for practical electron bunch sizes.

EOI's pulse compressors can be designed and built to attach to different types of UEDs and DTEMs, thus making them suitable for enhancing the study of the structure, composition, and bonding states of new materials at ultrafast time scales to advance material science research in the field of nanotechnology as well as biomedical research.

I. Phase I Technical Objectives.

The goal of this project is to establish the feasibility of an electron mirror-based pulse compressor that can be attached to new and retrofitted DTEMs and UED cameras to improve the temporal resolution of these instruments from the characteristic range of a few picoseconds to a few nanoseconds and beyond, into the sub-100 femtosecond range. The key feature of EOI's pulse compressor approach is the combination of a magnetic beam separator that does not introduce significant aberrations and an electron mirror, which can compress pulses with varying number of electrons and can be tuned to match different column geometries. This approach has three major advantages compared to existing pulse compressor designs [van Oudheusden, Chatelain, Kassier, Wang, Tokita]. First, this approach utilizes static electron-optical components to achieve the compression and thus does not suffer from the jitter problems encountered in the RF cavity approaches. Second, the use of a beam separator allows the compressor to be readily incorporated into the straight column axis of existing UED and DTEM instruments, thereby significantly simplifying the column alignment and improving its stability. The beam separator also allows the pulse to enter the electron mirror at normal incidence, which minimizes the aberrations introduced by the mirror. Third, the electron mirror provides the capability to correct the aberrations of the objective lens in the UED and DTEM instruments.

Technical Approach

The pulse compressor design utilizes an electrostatic electron mirror combined with a magnetic beam separator [Mankos[a,b]] to compress an electron pulse that has spread longitudinally from its initial duration of tens of femtoseconds at the source to picoseconds and beyond. A layout of the electron pulse compressor is shown in Fig. 1. Electrons emitted by the photocathode enter the beam separator and are deflected by 90 degrees off the beam axis towards the electron mirror. Higher energy electrons penetrate more deeply into the retarding field of the electron mirror, thereby experiencing a longer path length in the mirror. After reflection, the velocity distribution of the pulse is inverted, as the trailing edge of the pulse has a higher energy than the leading edge. The reflected electron pulse reenters the beam separator and is deflected by 90 degrees back into the main column axis. The inversion of the velocity distribution results in the temporal compression of the propagating pulse as the pulse moves toward the specimen.

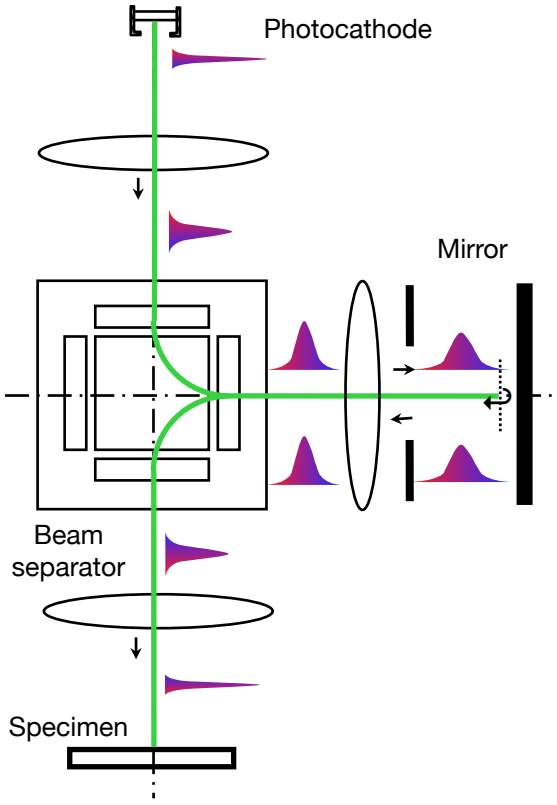

Figure 1. Pulse compressor principle.

In order to establish the feasibility of this novel instrumentation, Electron Optica focused the phase I research on six key objectives:

1. Review candidate architectures

Evaluate possible layouts including a variety of photocathodes guns, beam separators, electron mirrors and lenses by analyzing 1st order optics design options for the pulse compressor with aberration correction. Select the most promising UED and DTEM candidate for further analysis.

2. Establish temporal and optical properties of the electron mirror

Analyze the temporal and optical properties of the electrostatic electron mirror by simulating ray trajectories, time of flight, focal length, imaging properties, and aberrations up to 3rd order. Demonstrate

that the electron mirror can compress pulses with a varying number of electrons and achieve the requisite temporal resolution for a range of column lengths. Demonstrate that the mirror can offset the chromatic aberration coefficient of a typical UED or DTEM objective lens.

3. Establish optical properties of the magnetic beam separator

Analyze the optical properties of the magnetic beam separator by modeling focusing properties, energy dispersion, and aberrations. Optimize separator design for UED and DTEM instruments.

4. Evaluate impact of the Coulomb interactions

Combine the effect of Coulomb interactions with the optical aberrations to determine the temporal and spatial resolving power as a function of the number of electrons per pulse and of the beam energy. Carefully evaluate the Coulomb effects at the mirror, where the speed of the electron bunch goes to zero. Determine the range for the number of electrons/pulse and for the beam energy where the impact of Coulomb interactions does not significantly degrade the temporal and spatial resolutions.

5. Design UED column with mirror pulse compressor and aberration correction and establish its electron-optical parameters

Analyze the temporal and spatial resolutions of the complete column including the photocathode, the beam separator, the electron mirror, and the lenses. Derive the electron-optical parameters of the UED column including the pulse compressor and the aberration corrector.

6. Design DTEM column with mirror pulse compressor and aberration correction and establish its electron-optical parameters

Analyze the temporal and spatial resolutions of the complete pulse compressor including the photocathode, the two beam separators, the two electron mirrors, and the lenses. Derive the electron-optical parameters of the DTEM column including the pulse compressor and the aberration corrector.

II. Phase I Accomplishments.

The following section describes the results and the activities performed during phase I that were required to remove the technical risks and to validate the novel concepts described in the previous section. The results are grouped into six tasks, matched to the six technical objectives discussed in the previous section.

Task 1. Review candidate architectures

The geometry of the pulse compressor and its main electron-optical components, i.e. the electron source, the beam separator, the electron mirror, and the electron lenses (condenser, transfer and the objective) are shown in Fig. 2. Electron sources most commonly used in UEDs and DTEMs utilize photo-electron emission from metal photocathodes, typically Cu or W, which produce an ultrafast electron pulse with an initial pulse width in the range of 1 to 100 femtoseconds.

After the initial pulse formation, repulsive Coulomb interactions between the electrons broaden the temporal and spatial extent of the pulse during the travel to the specimen. A large fraction of the Coulomb broadening occurs near the cathode surface before the electrons are accelerated to the beam energy. The Coulomb broadening at the mirror turnaround point, where the electrons are decelerated to zero energy, is negligible in comparison because the beam envelope in the mirror is carefully designed to minimize Coulomb interactions by spreading the pulse in both the longitudinal and transverse directions.

The Coulomb effects mainly increase the beam energy spread (Boersch effect) from a fraction of an electron-Volt to hundreds or even thousands of electron-Volts. The Boersch effect has a two-fold impact on the electron optics: it spreads the arrival time window of the pulse from tens of femtoseconds to picoseconds; and it increases the objective lens chromatic aberration, which reduces the spatial resolution from Ångstroms to nanometers. The spread in the arrival time window is due to the path difference between electrons with energies E_{min} and E_{max}. Defining d as the distance between the mirror and the

photocathode

$$d = L_i + L_1 + L_2,$$

the electron with the lowest velocity lags behind the highest by $\Delta s_v = d\,(1 - v_{min}/v_{max})$. Using the non-relativistic relation between the speed v and the kinetic energy eU,

$$1 - v_{min}/v_{max} \approx \Delta U/2U,$$

with $eU = E_{min}$ and $e\Delta U = E_{max} - E_{min}$, and $\Delta U \ll U$, the path difference due to energy spread is approximated as

$$\Delta s_v = d \cdot \Delta U/2U.$$

For a pulse with a nominal energy eU of 100 keV, an energy spread $e\Delta U$ of 1000 eV, and a geometry with practical dimensions of L_i = 300 mm, L_1 = 75 mm and L_2 = 300 mm, the path difference is found to be $\Delta s_v \approx$ 3.4 mm, which corresponds to a temporal spread of about 18 picoseconds (the relativistic correction is of the order U/mc^2 or 20%).

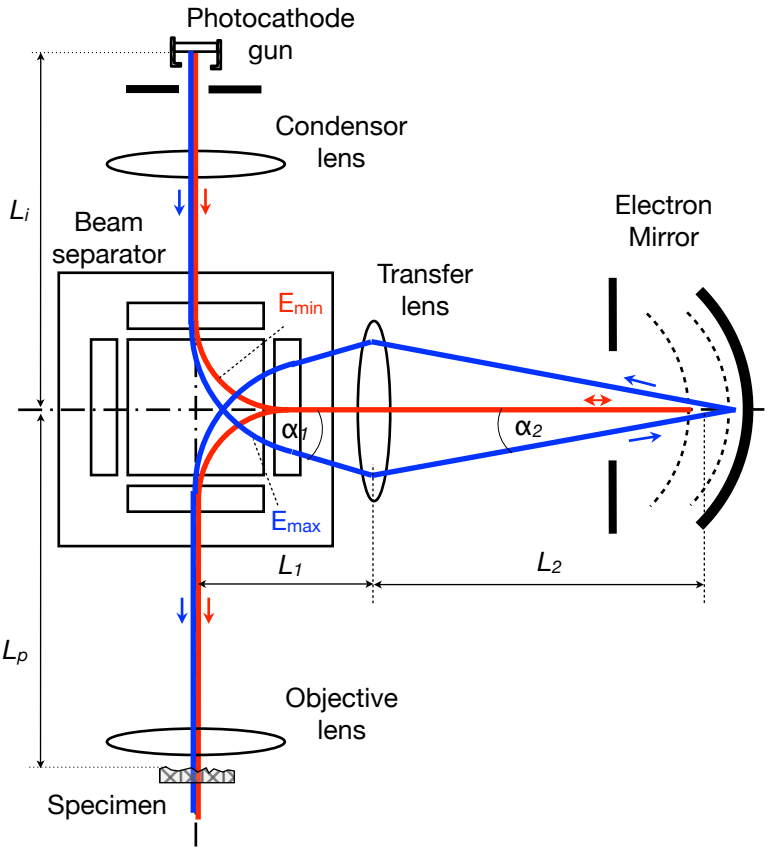

Figure 2. Pulse compressor geometry.

The condenser and the transfer lens are tuned to form a magnified image of the emission spot onto the mirror plane. The beam separator acts as a field lens that deflects the electron pulse by 90 degrees off the beam axis towards the electron mirror. The beam separator also disperses the electrons according to their energies. A typical separator geometry with an overall dimension of 100 mm x 100 mm disperses a beam of electrons with a nominal energy of 100 keV by $D \sim 0.5$ µm/V at the dispersion plane, which is located at the transfer lens. The dispersion will also introduce a path difference between the low and high energy electrons; however, this path difference is found to be negligible as approximated by

$$\Delta s_D \approx (1/L_1 + 1/L_2)(D\,\Delta U)^2/2.$$

For an energy spread of $e\,\Delta U$ =1000 eV, and a 100 mm x 100 mm beam separator, Δs_D is just 2 µm.

The mirror compresses the pulse by providing an energy dependent turning point. High energy electrons penetrate more deeply into the retarding field of the electron mirror, resulting in the path difference

$$\Delta s_m = \Delta U / E_m$$

with E_m equal to the electric field at the turning point. Upon reflection, this path difference doubles. Assuming for simplicity that the specimen is located at a distance $L_p = L_i$ from the beam separator, the condition for pulse compression at the specimen is accomplished by setting

$$\Delta s_v = \Delta s_m.$$

Any asymmetry due to $L_p \neq L_i$ or due to Coulomb effects in the second leg can be accommodated by adjusting the mirror electric field from

$$E_m \approx 2U / d.$$

With d =675 mm and U =100 kV, an electric field of 0.3 kV/mm is needed at the turnaround point. It is important to note that the electric field E_m is independent of the energy spread ΔU. Hence, once the mirror is set up for a bunch with a given number of electrons and thereby a given Coulomb spread, there is no need to retune the mirror for a larger or smaller electron bunch.

The prism-mirror combination can be simultaneously exploited for the correction of the objective lens aberrations. Conventional, rotationally symmetric electron lenses strongly focus electron rays with larger entrance slopes and lower energies, resulting in positive spherical and negative chromatic aberration coefficients (Fig. 3). Electron mirrors, on the other hand, can be adjusted to focus the aforementioned rays more weakly, thus yielding tunable spherical and chromatic aberration coefficients with opposite signs that can be used to compensate the objective lens aberrations. Schmidt and Tromp utilized a tetrode mirror [Schmidt, Tromp, Preikszas] that eliminates both the chromatic and spherical aberration of the objective lens to improve the spatial resolution of a low energy electron microscope. More recently, we have proposed a novel electrostatic pentode mirror [Mankos[a]] that can further improve the resolution by correcting the 5th order spherical aberration.

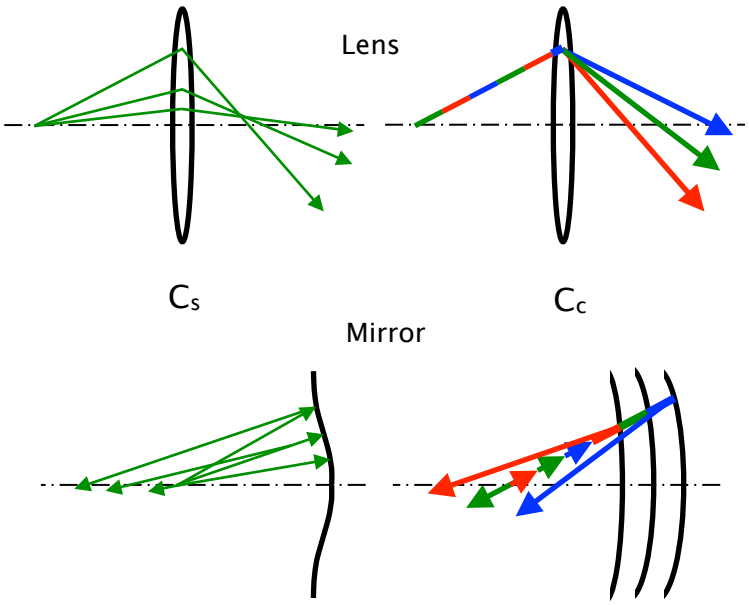

Figure 3. Lens aberrations and their correction using an electron mirror.

In a UED instrument, the aberration corrector is implemented in the same electron mirror that performs the temporal compression. The equipotential distribution in the electron mirror is tuned to not only provide the axial field distribution needed to invert the velocity distribution of the pulse, but also produce aberration coefficients that can compensate the objective lens aberrations. These corrections will become increasingly beneficial as the illuminated area is reduced for carrying out ultrafast diffraction experiments from small regions of the sample, e.g. from individual grains or nanoparticles.

In DTEM, the aberration corrector must follow the sample and objective lens, and thus cannot be combined with the pulse compressor, which precedes the sample. Here, a separate prism-mirror system must be placed in the projection optics of the DTEM column (see task 6). Electrons scattered by the sample enter the beam separator and are deflected by 90 degrees off the beam axis towards the electron mirror. The electron mirror is then tuned to cancel the combined aberrations of the objective lens, as well as the aberrations from the intermediate transfer and field lenses. The aberration-corrected beam is then

deflected back towards the screen.

Task 2. Establish temporal and optical properties of the electron mirror

The electron-optical properties of the electron mirror are key for the reversal of the velocity distribution and thereby for the downstream compression in the pulse before it impacts the specimen. The geometry of a pentode electron mirror composed of five rotationally symmetric electrodes is shown in Figure 4. The anode (entrance) electrode is grounded (V_5 = 0 V) while the last electrode is biased at a potential V_1 that is slightly more negative than the photocathode to reflect the electron beam. The incoming electrons with a higher energy (blue line) penetrate deeper into the electron mirror before they are reflected, resulting in a longer beam path in the mirror, while electrons with a lower energy (red line) are reflected earlier. Once the electrons leave the mirror, the faster electrons catch up with the slower ones until a temporal focus is established at a certain drift distance from the mirror.

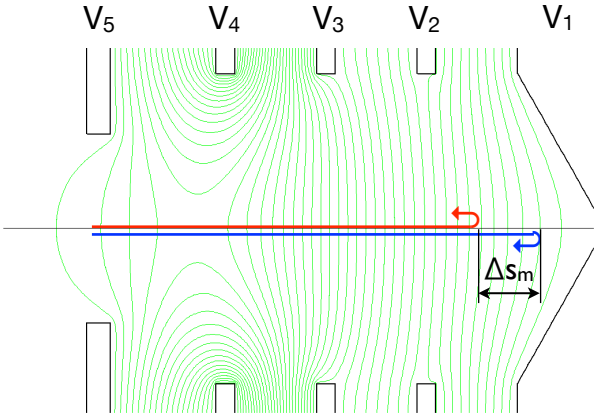

Figure 4. Equipotential distribution in a pentode mirror.

The potential V_4 is needed for focusing the beam. The potentials of the three inner electrodes provide the three knobs to tune the path differential Δz between the slowest and the fastest electrons in the pulse and to correct the spherical and chromatic aberration coefficients of the objective lens. The tuning capability is described for a particular field configuration in the pentode mirror, whose axial potential is shown in Fig. 5. As shown in Fig. 5a, the potential of the last mirror electrode is biased negatively with respect to

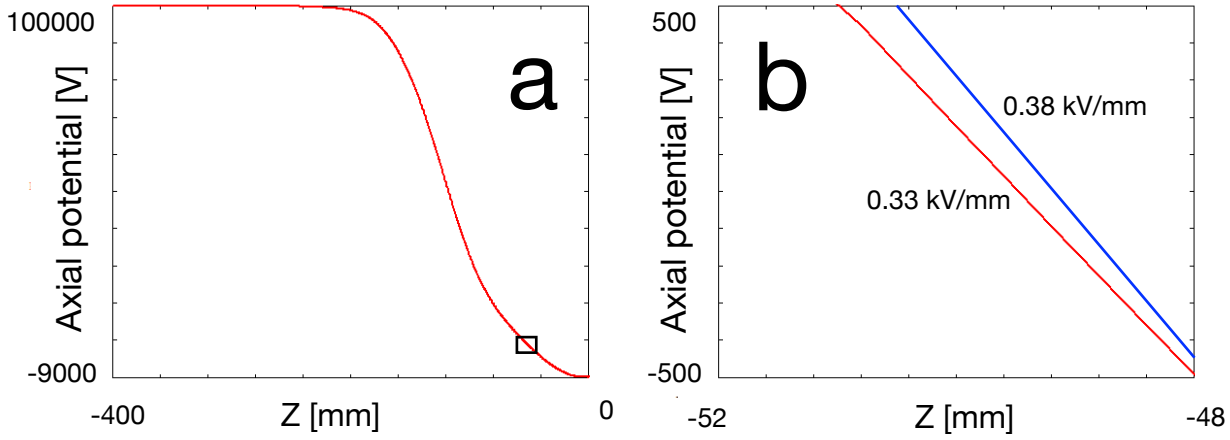

Figure 5. Overall axial potential distribution in the pentode mirror (a) and the local axial potential distribution near the turn-around point (b).

the electron source by 9000 V, while the neighboring electrode is biased positively with respect to the electron source by 9000 V. The region near the turnaround point with a potential near 0 V is marked by the rectangle in Fig. 5a and enlarged in Fig. 5b. With the above bias setting, a local electric field of 0.33 kV/mm is achieved (red line). A slight increase in the relative bias to ±10000 V (blue line) increases the local electric field to 0.38 kV/mm. Therefore, by varying the potential on the last two electrodes, the electric field at the turn-around point may be fine-tuned to adjust the position of temporal focus downstream.

The geometry of the mirror electrodes as well as the potentials applied to the individual electrodes can be further tailored to tune the aberrations of the electron mirror over a wide range [Schmidt, Tromp]. A pentode mirror, as shown in Fig. 4, can be used to compensate the leading 3rd order spherical aberration, the 2nd rank chromatic aberration, and the 5th order spherical aberration of a LEEM objective lens to a fraction of 1 % [Mankos[a]].

The specialized software package MIRROR DA developed by MEBS, Ltd. was used for the analysis of the electron mirror optics. This differential algebra-based (DA) software package computes the temporal and optical properties, including aberrations of any order, for electron mirrors with any symmetry and can handle combinations of electron mirrors and electron lenses in a unified way. Results computed with MIRROR DA were shown to be in good agreement with those extracted by direct ray tracing with relative deviations of less than 0.065% for all primary aberration coefficients [Munro].

A high-quality objective lens with an object-side spherical (C_{so}) and chromatic (C_{co}) aberration coefficient of 1 mm with magnification M yields an image-side spherical aberration coefficient of $C_{si} = M^4 C_{so}$ and a chromatic aberration coefficient of $C_{ci} = M^2 C_{co}$. The aberration corrector must cancel the two aberration coefficients at the image plane, which for typical magnification ratios of 5-20, are in the range of 625 mm - 16 m and 25 mm - 400 mm, respectively. The ability to tune the aberration coefficients of the pentode mirror is demonstrated in Fig. 6, which plots the mirror's aberration coefficients as a function of the potential on the central electrode V_3. Fig. 6a demonstrates that the spherical and chromatic aberration coefficients of the pentode mirror can be tuned into the aforementioned range for a range of electric fields at the turn-around point. Fig 6b demonstrates that the two aberration coefficients can also be tuned while maintaining a constant electric field at the turn-around point. This is achieved by maintaining the difference between V_1 and V_2. In the example shown in Fig. 6b, the chromatic aberration coefficient can be chosen to equal 100 mm, while the spherical aberration coefficient can be tuned from 6 to 10 m by varying the potentials V_1 and V_2 together by ±1 kV.

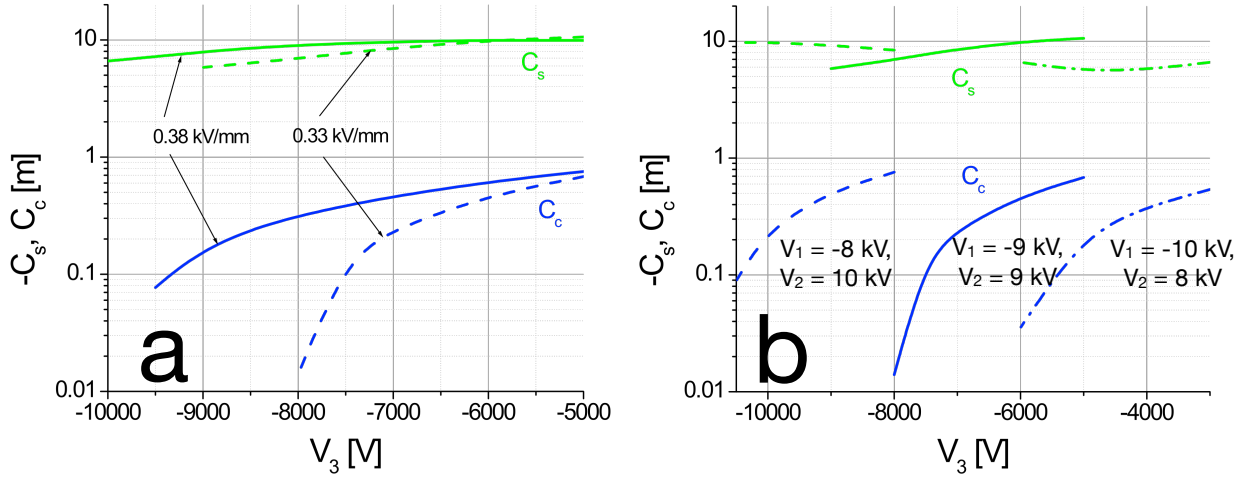

Figure 6. Spherical and chromatic aberration coefficients of a pentode mirror vs. potential V_3: a - for different electric fields at the turn-around point, b - for different common-mode potentials on the last two electrodes.

Task 3. Establish optical properties of the magnetic beam separator.

The beam separator is based on a magnetic prism array, a proven and reliable design, which has been developed for low energy electron microscopes (LEEMs) to separate the otherwise overlapping illumination and projection optics [Mankos[b]]. The electron-optical properties of this beam separator strongly impact the design of the entire pulse compressor as the separator geometry is central to defining

the image and dispersion planes.

The optical properties of simple magnetic prisms (Fig. 7) differ considerably in the plane that cuts across the top and bottom magnetic plates (the vertical plane) and the plane that separate these two plates (the horizontal or mid-plane), giving rise to large astigmatism and distortion. For the pulse compressor, the magnetic prism needs to concurrently provide a deflection of 90° while behaving as a round lens overall in order to preserve the quality of the illuminating beam. This behavior can be achieved in a beam separator that is composed of a close-packed magnetic prism array [Kolarik, Degenhardt, Mankos[b]]. Figures 7a and b show an example of such an array consisting of a large, central square region with a uniform magnetic field that connects the top and bottom plates, surrounded by several smaller sectors with individual coils to locally modify the magnetic field. The strengths of these fringe fields are tuned to match the focus in the vertical plane with that achieved naturally by the curvature in the path in the mid-plane.

PRISM, a proven software package developed by MEBS, Ltd. was used to calculate the electron-optical properties of 90° prism array configurations. In this package, prism arrays comprising magnet regions held at different magnetic excitations and separated by gaps consisting of grooves can be evaluated. The two-dimensional fields in the prism are calculated by a conformal mapping technique known as the Schwartz-Christoffel transformation. The software computes the optical axis, the multipole field components along the optical axis, the first order (paraxial) trajectories, the locations of the image planes, and the dispersion and the primary (second rank) geometrical and chromatic aberrations in these planes. Trajectories are also computed by direct ray-tracing via a Runge-Kutta solution of the equations of motion to assess the full spot size at the dispersion plane, which is a result of the convolution of the magnified source size at the crossover with the primary and higher-order aberrations of the prism.

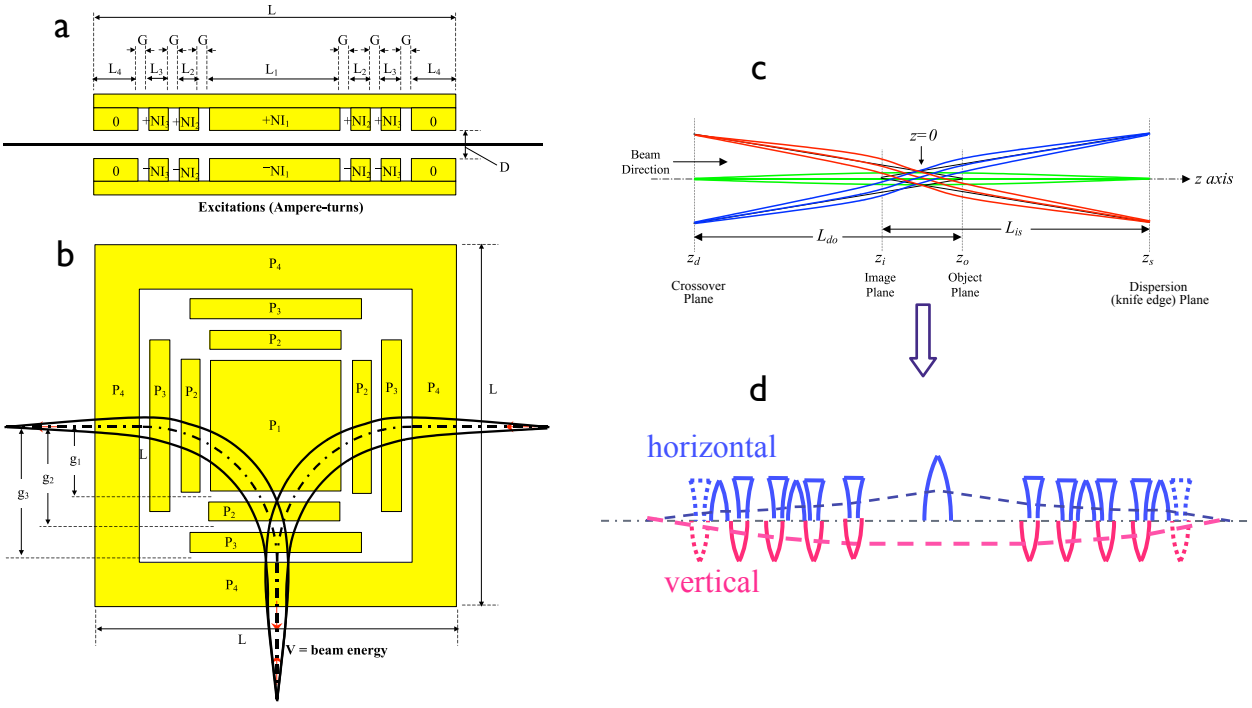

Figure 7. Magnetic prism array layout: a - cross-sectional view, b - mid-plane view, c - unfolded ray diagram along the curved beam axis, d - equivalent optical model along the unfolded axis.

The optical effects of the magnetic field in each sector and in the transition between sectors can be represented by a convex or a concave lens with disparate properties in the horizontal and vertical planes. As illustrated in Figs. 7c and 7d, each 90° deflection is thus a complex optical assembly that needs to be carefully optimized. In the simulations, the geometry of the individual sectors, the total number of

sectors, as well as the individual sector excitations were varied in order to achieve the desired energy dispersion with a practical beam separator design.

We have selected a compact separator design for UEDs and DTEMs operating at beam energies of 20-100 keV that utilizes a magnetic prism array with an overall size of 100 mm x 100 mm, as shown in Fig. 8. This design produces a dispersion of 2.6 µm/V at 20 keV and 0.52 µm/V at 100 kV. The dispersion plane is located only 105 mm from the center, which makes for a short column, an important factor for minimizing Coulomb interactions.

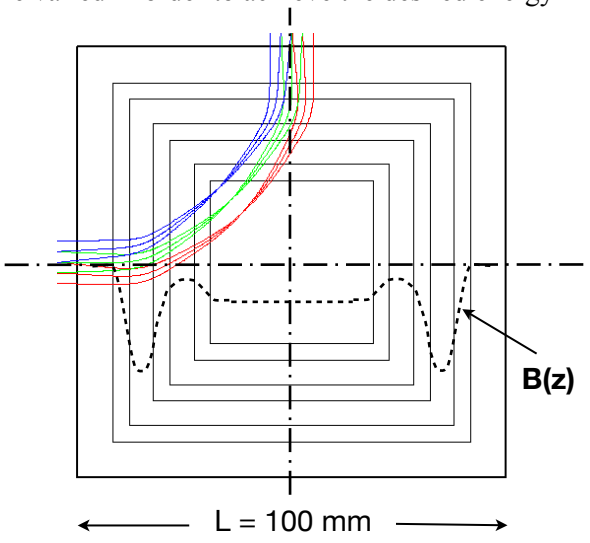

Figure 8. Layout of compact magnetic beam separator for 20-100 keV.

Task 4. Evaluate impact of the Coulomb interactions

Many of the intended applications in UED and DTEM are aimed at operating in the single-shot mode, and thus require a large number of electrons per pulse. A 10 femtosecond pulse with 10^4 electrons per pulse generates high space charge densities with a peak current of 160 mA, which inevitably results in large Coulomb interactions. Coulomb interactions can negatively impact the pulse compressor properties by introducing temporal blur from the increasing energy spread (Boersch effect) and by introducing spatial blur from trajectory displacement (Loeffler effect) as well as space charge defocus [Jansen]. The temporal blur can be reversed for uniformly charged ellipsoidal electron bunches such as the ones produced by femtosecond laser photoemission [Siwick]. The space charge determined by the averaged charge density defocuses the beam in the Gaussian plane and changes the image magnification. The defocus can be corrected for a uniform charge distribution in an axially symmetric beam by refocusing the lens [Mkrtchyan]. However, the stochastic nature of the Boersch and Loeffler effects preclude their correction. These effects increase the energy spread and reduce the beam brightness, both of which further deteriorate the spatial resolution of the optics.

The IMAGE software package from MEBS Ltd. was used to evaluate the impact of Coulomb interactions. The software package computes electron-optical properties by propagating bunches of particles through realistic electromagnetic fields by accurate direct ray-tracing and captures the combined effect of Coulomb interactions and aberrations. The resulting energy spread and beam blur were calculated for electron pulses with an initial pulse width of 10 femtoseconds and the number of electrons per pulse ranging from 10 to 10,000, corresponding to a range of initial pulse currents from 160 µA to 160 mA. The simulation is divided into two steps. First, the Coulomb interactions in the illumination optics are simulated. Here, the electrons start with an initial energy spread of ~ 0.5 eV at the photocathode surface and are accelerated in the electron gun to the beam energy of 100 keV with which they travel through the condenser lens, the beam separator, and the transfer lens to the mirror entrance. This simulation allows us to characterize the pulse shape and width at the mirror entrance and define the parameters needed to tune the electron mirror for pulse compression. Second, the Coulomb interactions in the electron mirror are simulated. The IMAGE software cannot propagate the pulse at a point of reflection. Hence, the electrons are started from rest at the mirror reflection plane and are traced back to the center of the beam separator. The contribution that is not simulated, that from the entrance to the mirror, will at most double the Coulomb blur found.

In order to simulate the Coulomb effects in the illumination arm with the IMAGE code, the column is approximated with a straightened optical axis with the equivalent length. The beam separator is modeled as a magnetic field lens that images the dispersion plane with unit magnification and with a focal length that is given by the overall focusing strength of the beam separator along the unfolded axis (Figs. 7d). The gradual increase in the energy spread and the beam blur at the mirror entrance plane with the

increasing electrons per pulse in the illumination optics is illustrated in Fig. 9.

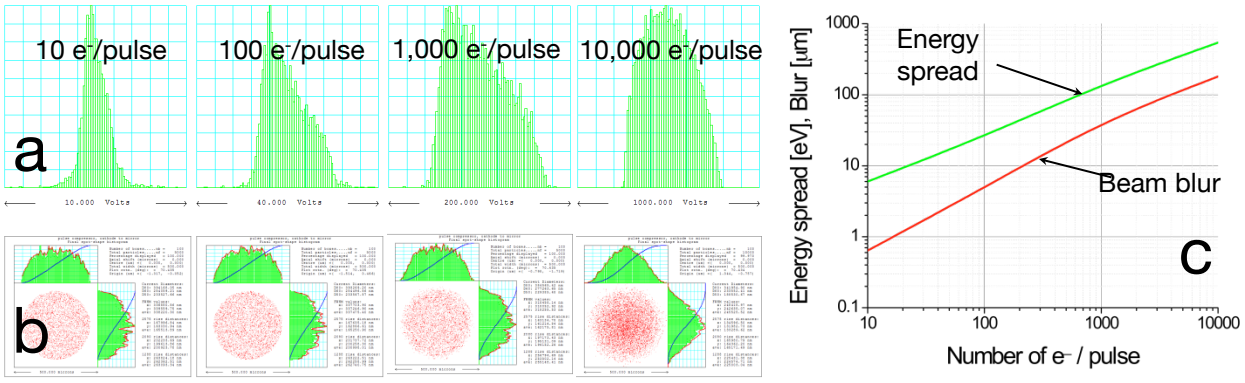

Figure 9. Pulse characteristics at mirror entrance plane for varying number of electrons/pulse, a - energy distribution, b - spatial distribution, c - energy spread and beam blur at 100 keV beam energy.

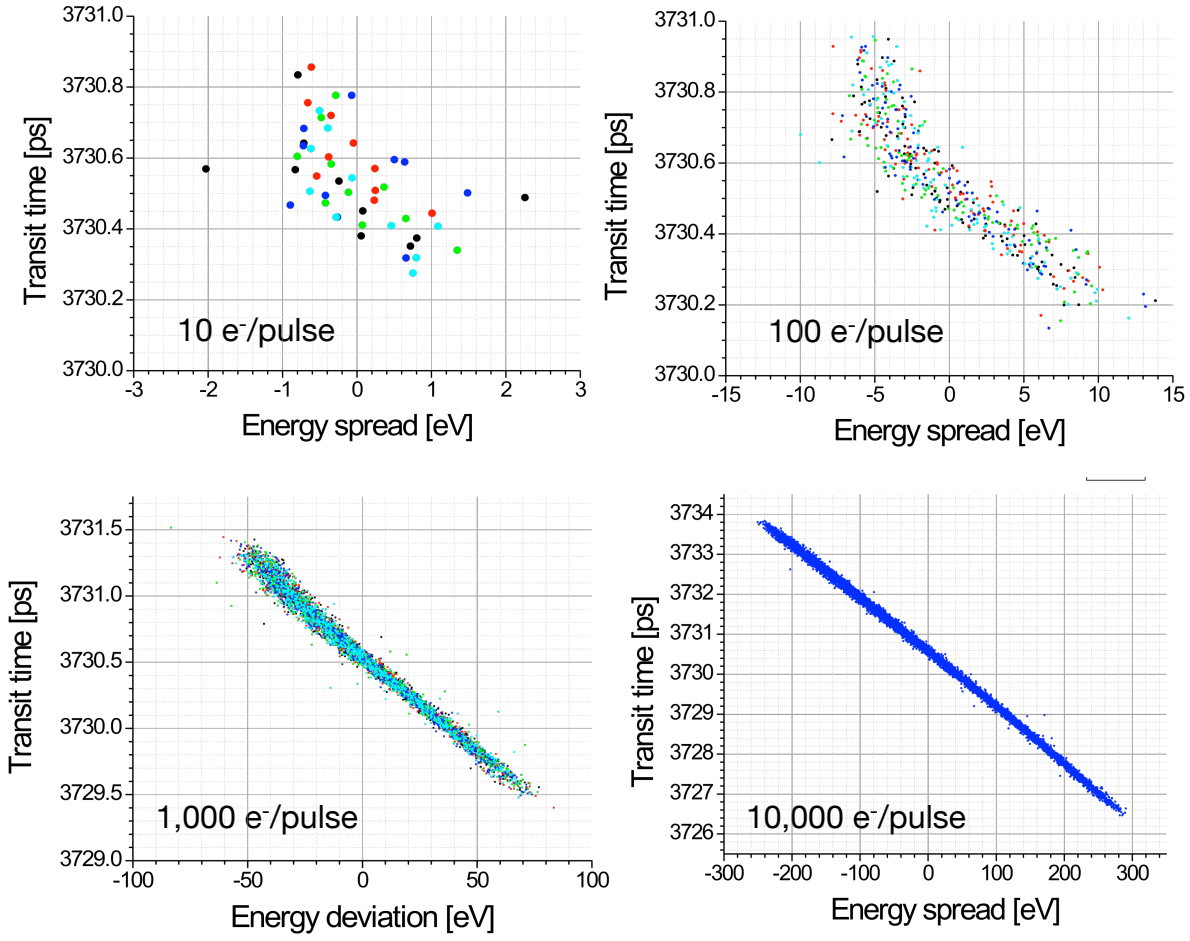

Figure 10a. Pulse transit time versus energy spread at mirror entrance plane for a varying number of electrons/pulse, showing 5 pulses with 10-1,000 e⁻/pulse, and 1 pulse with 10,000 e⁻/pulse.

The dependence of the pulse transit time on the energy spread (Fig. 10a) displays the characteristic linear chirping generated by the femtosecond laser stimulated photoemission [Siwick, van Oudheusden]. The temporal spread of the chirped distribution in the low energy tail of the pulse is broader by approximately 2x when compared to the high energy tail, resulting in a characteristic 'dagger'-like pulse shape. The full width of the temporal spread across a small energy interval is approximately 200 femtoseconds, due to the initial thermal spread and the stochastic contribution of the Coulomb interactions.

A close examination of the transit time of the individual electron pulses over a small energy spread window reveals another interesting and somewhat counterintuitive feature, as demonstrated in Fig. 10b. The temporal spread of the pulse distribution over a small interval in energy spread (e.g. 1 eV) appears to decrease with an increasing number of electrons/pulse, producing a distribution that is much more tightly packed. This suggests that pulse widths with a FWHM of 100 femtoseconds or less should be achievable, in particular for pulses with a larger number of electrons/pulse.

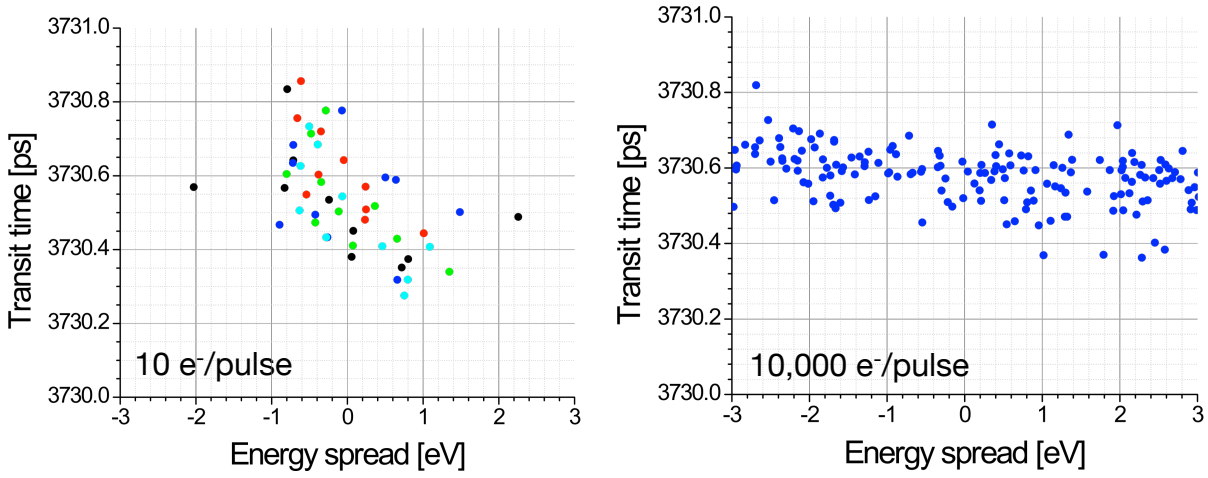

Figure 10b. Pulse transit time versus energy spread at the mirror entrance plane for a 10 and 10,000 electrons/pulse.

Coulomb interactions in the electron mirror, exacerbated by the fact that electrons slow down and turn-around at the reflection plane, have the potential to negatively impact the pulse compression. In order to minimize this effect, the illumination optics was designed to minimize the current and current density at the mirror reflection plane. The initial Coulomb interactions, at the cathode, spread the arrival time window of the pulse at the mirror from ten femtoseconds to picoseconds, which reduces the current (and current density) by more than 2 orders of magnitude, depending on the number of electrons/pulse. Furthermore, the image at the mirror reflection plane is enlarged by a factor of 4, which reduces the current density by another factor of 16. For a 10,000 electrons/pulse, the current thus drops from 160 mA at the photocathode surface to ~ 210 μA at the mirror reflection plane, while the current density drops from ~ 2000 A/cm^2 to less than 2 A/cm^2.

For simulating the Coulomb interactions in the mirror, the electrons are started from rest at the mirror turnaround plane with the beam current and energy spread obtained from the first simulation step and propagated through the transfer lens to form a demagnified image at the center of the beam separator. As this simulation accounts only for one pass through the mirror, the net impact of the mirror should be less than or equal to twice the effect of a single pass. Figures 11 and 12 show that the impact of Coulomb interactions in the mirror is quite small, a result of the reduction in the current density in the illumination optics. For pulses with 10 to 10,000 electrons, the width of the energy distribution derived from the initial histogram at the mirror and the final histogram at the beam separator differ on the order of a few % (Fig. 11). The difference between the initial and final spatial distribution of these pulses (Fig. 12) is also

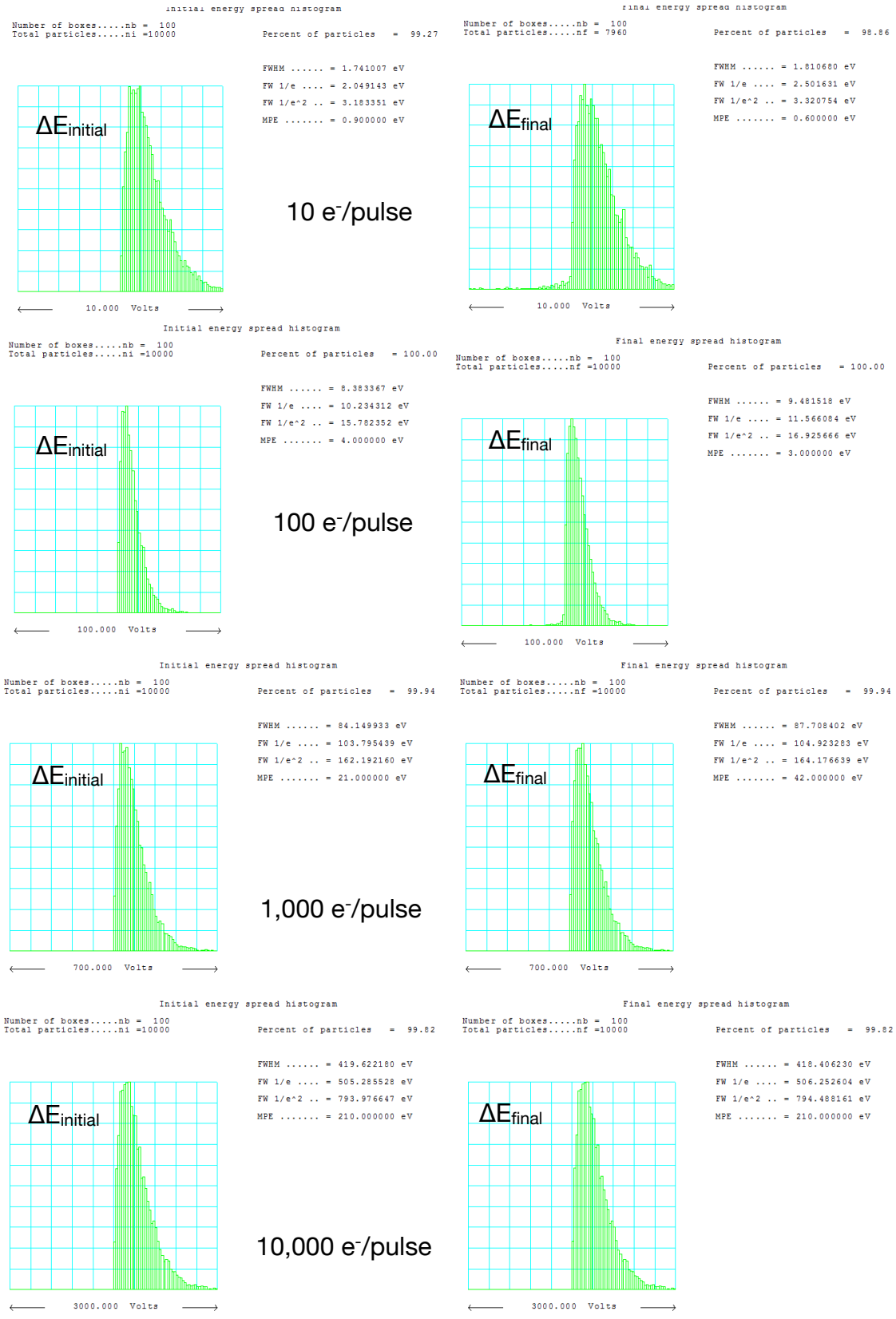

Figure 11. Initial and final energy histograms for a range of 10 to 10,000 electrons/pulse travelling from the mirror to the beam separator.

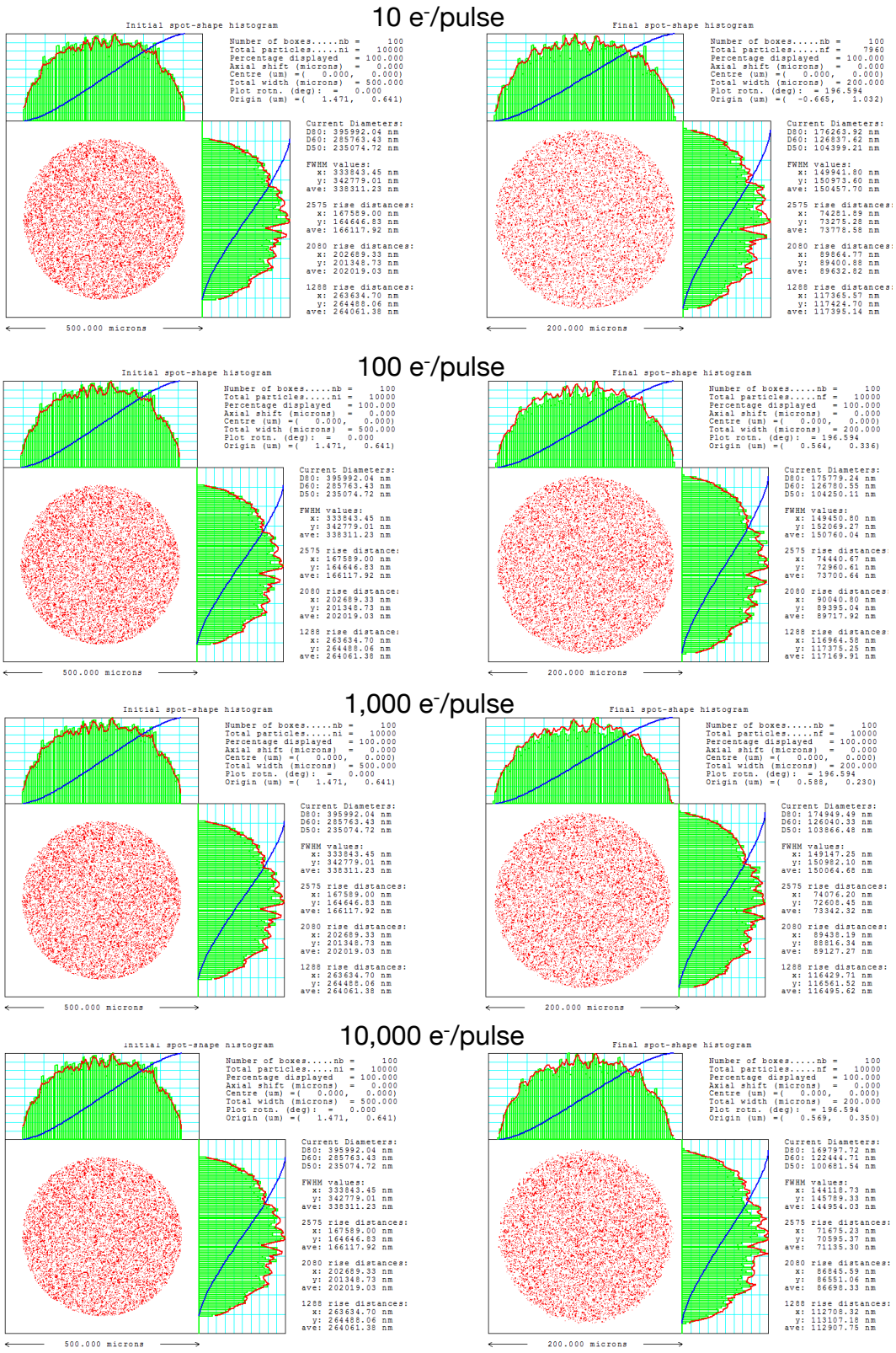

Figure 12a. Initial (left) and final (right) spatial distribution for a range of 10 to 10,000 electrons/ pulse travelling from the mirror to the beam separator.

minuscule, producing a change in the beam blur (Fig. 12b) that is approximately 2 orders of magnitude smaller than that for the illumination optics (Fig. 9c).

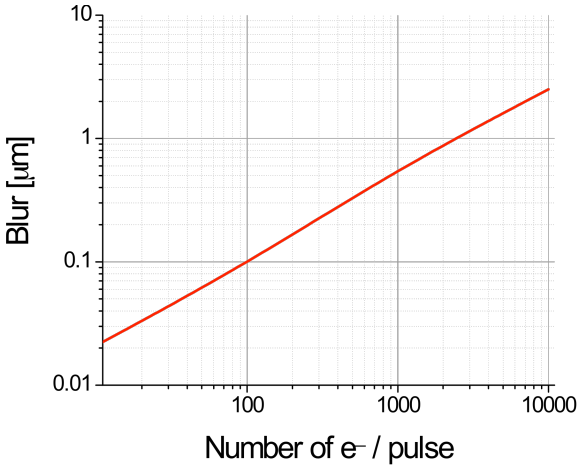

Figure 12b. Spatial blur for a range of 10 to 10,000 electrons/pulse travelling from the mirror to the beam separator.

Task 5. Design UED column with mirror pulse compressor and aberration correction and establish its electron-optical parameters

In this design step, the results obtained from simulating the optical properties of the electron mirror, the beam separator, and the Coulomb interactions were folded into a complete model describing the key electron-optical parameters of the UED outfitted with a pulse compressor. A ray diagram of the complete UED system and its conceptual mechanical layout with a column length of 600 mm is shown in Fig. 13. Electrons emitted by the photocathode are focused by the condenser lens to form a magnified image at the center of the beam separator, while a crossover is formed in front of the beam separator. The beam separator, a magnetic prism array, deflects the beam off the UED column axis by 90 degrees towards a module with a transfer lens and an electron mirror. The beam separator images the beam spot onto itself, with +1x magnification, while the crossover is magnified at the exit dispersion plane with -1x magnification. The transfer lens, located at the exit dispersion plane, further magnifies the beam spot at the mirror's reflection plane, thereby reducing the Coulomb interactions. The mirror compresses the

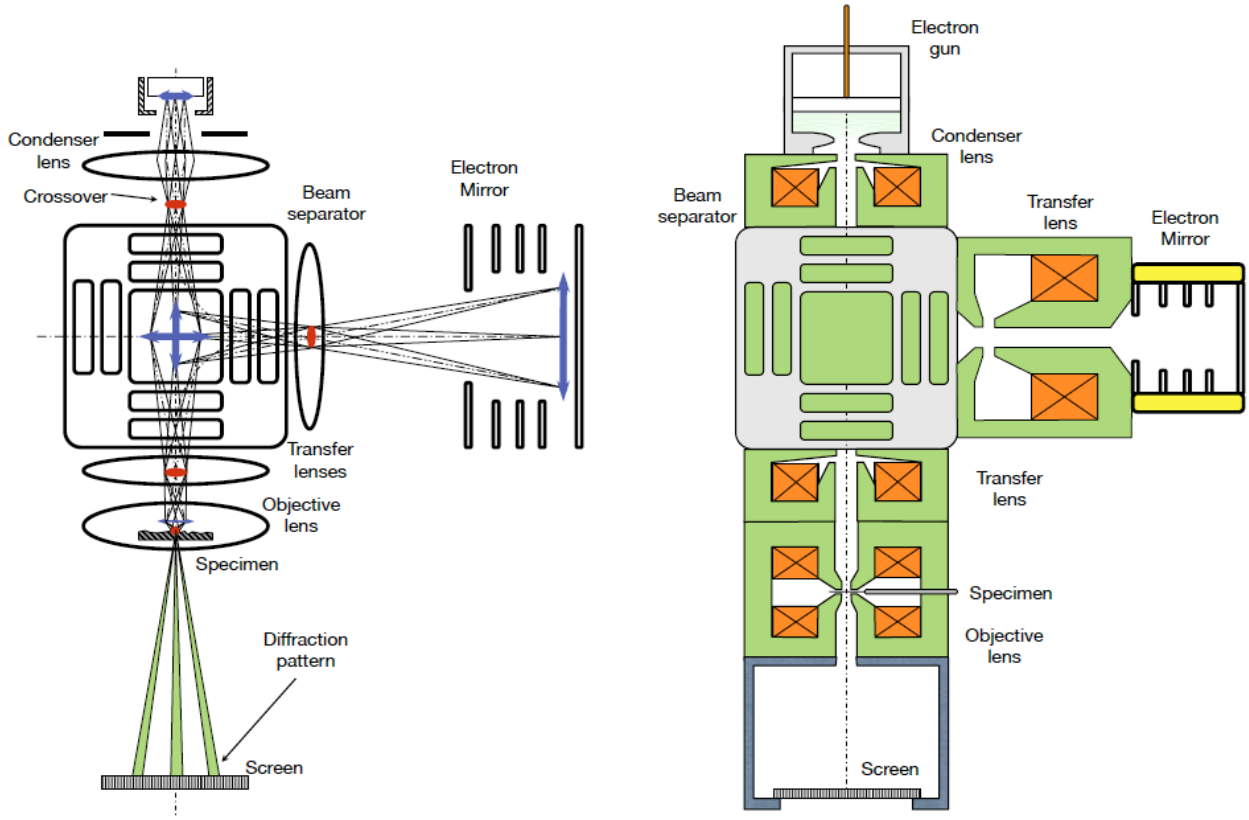

Figure 13. Ray diagram (left) and conceptual mechanical column layout of a UED camera with a mirror pulse compressor.

pulse by providing an energy dependent turning point. High energy electrons penetrate more deeply into the retarding field of the electron mirror, resulting in a path difference that is inversely proportional to the electric field at the turning point. The electric field and the overall potential distribution of the electron mirror is tuned to achieve pulse compression once the beam strikes the sample, while simultaneously canceling the chromatic and spherical aberration of the objective lens. After reflection, the beam spot is demagnified at the center of the beam separator, deflected once more by 90 degrees, and transmitted back into the center of the beam separator with +1x magnification, while the crossover is transmitted with -1x magnification at the exit dispersion plane. Due to the symmetry introduced by the mirror, the dispersion introduced by the double passage through the beam separator is cancelled. A transfer lens located at the crossover plane demagnifies the beam spot onto the objective lens, which in turn greatly demagnifies the crossover at the specimen plane to form a small illumination spot. Electrons scattered by the sample form a diffraction pattern that is then observed downstream on a viewing screen.

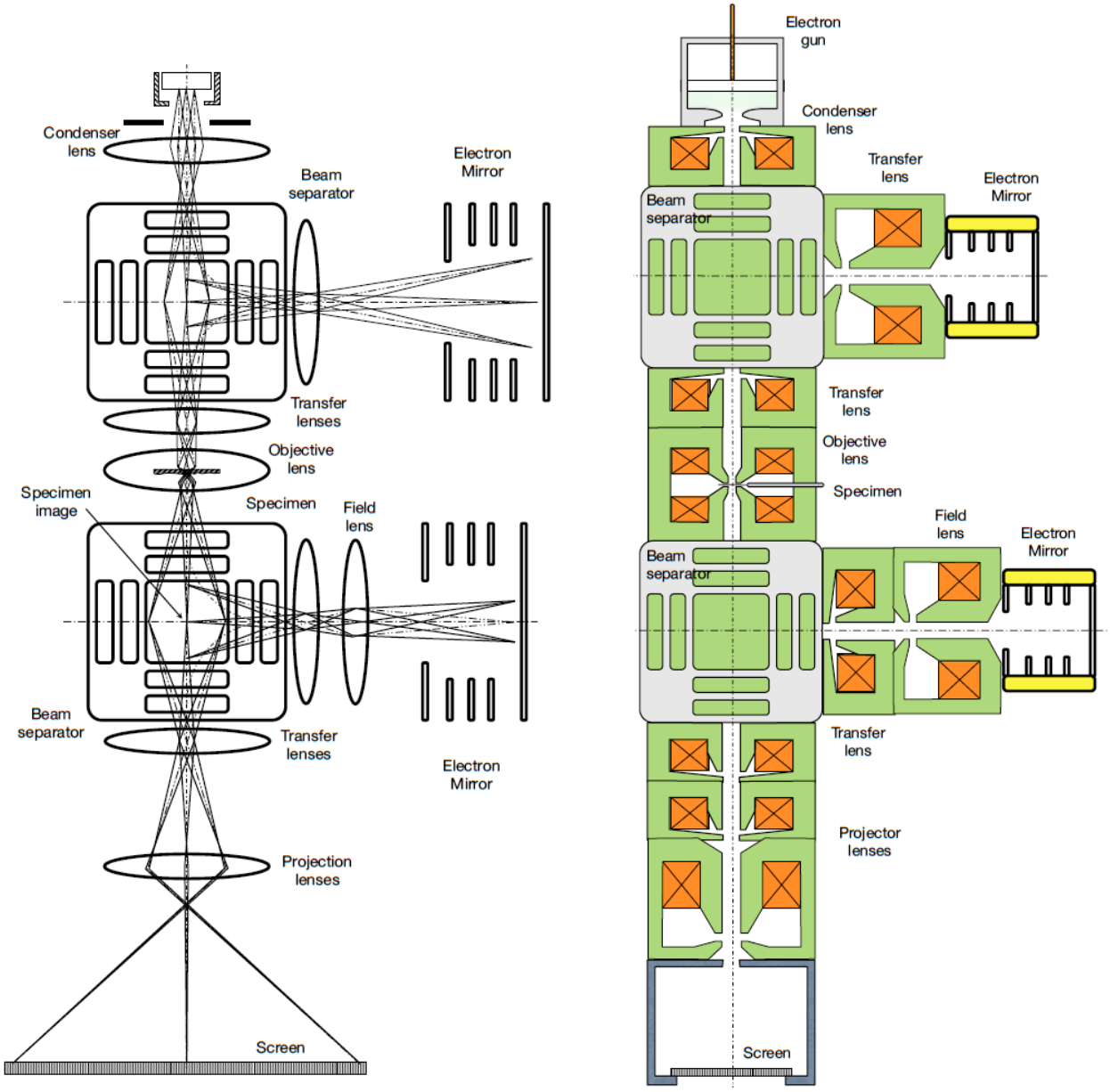

Figure 14. Ray diagram (left) and conceptual mechanical column layout of a DTEM with a mirror pulse compressor.

Task 6. Design DTEM column with mirror pulse compressor and aberration correction and establish its electron-optical parameters

In this design step, the results obtained from simulating the optical properties of the electron mirror, the beam separator, and the Coulomb interactions were folded into a complete model describing the key electron-optical parameters of the DTEM outfitted with a pulse compressor. In DTEM, the aberration corrector must follow the sample and objective lens, and thus cannot be combined with the pulse compressor, which precedes the specimen. The aberration corrector is based on a second beam separator-electron mirror combination and is inserted in the projection optics of the DTEM column (Fig. 14), following the specimen. The specimen illumination and pulse compression is performed exactly the same way as in a UED camera as described in the previous section. Electrons scattered by the sample form a specimen image which is magnified by the objective lens at the center plane of the second beam separator. A transfer lens refocuses the specimen image onto the object plane of the electron mirror. The electron mirror images the object onto itself, without forming an intermediate image in the mirror. A field lens is placed at the mirror object plane to control the field rays. The electron mirror is then tuned to cancel the aberrations of the objective lens, as well as the aberrations from the intermediate transfer and field lenses. The aberration-corrected beam is refocused at the achromatic center plane of the second beam separator, which deflects the beam back towards the main column axis. After the second deflection by the second beam separator, the aberration-corrected image is transported into the projection optics and magnified on a viewing screen.

III. Significance of Phase I Results.

In Phase I, we successfully demonstrated that the proposed mirror pulse compressor can reduce the temporal spread of a pulsed electron beam into the 100 femtosecond regime. Detailed electron-optical analysis of the pulse compressor system and its key components were performed using state-of-the-art simulation software, yielding an optical design that is suitable for a pulse compressor prototype. We have completed all the tasks and have met the milestones outlined for Phase I. The key risks have been retired, and Electron Optica is now ready to embark on building the prototype in Phase II.

IV. Bibliography & References Cited

Chatelain, R. P., V. Morrison, C. Godbout, and B. J. Siwick, Ultrafast electron diffraction with radio-frequency compressed electron pulses, Appl. Phys. Lett. 101 (2012), p. 081901.

Degenhardt, R., Korrektur von Aberrationen in der Teilchenoptik mit Hilfe von Symmetrien, Ph.D.Dissertation (1992), Technische Hochschule Darmstadt.

Grzelakowski, K.P., Tromp, R. M., Temporal and Lateral Electron Pulse Compression by a Compact Spherical Electrostatic Capacitor, Ultramicroscopy 130 (2014), p. 36-43.

Jansen, G.H., Trajectory displacement effect in particle projection lithography systems: Modifications to the extended two-particle theory and Monte Carlo simulation technique, J. Appl. Phys. 84 (1998), p. 4549.

Kassier, G. H., Haupt, K., Erasmus, N. , Rohwer, E. G., Schwoerer, H., Achromatic reflectron compressor design for bright pulses in femtosecond electron diffraction, J. Appl. Phys. 105, (2009), 113111.

Kolarik, V., Venklasen, L.H., Mankos, M., Close packed prism arrays for electron microscopy, Optik 87 (1991), p. 1-12.

Mankos[a], M., K.Shadman, H.H.J.Persson, A.T.N'Diaye, A.K.Schmid, R.W.Davis, Ultramicroscopy 145, 36-49 (2014).

Mankos[b], M., Adler, D., Veneklasen L., Munro, E. , Electron optics for high throughput low energy electron microscopy, Surface Science 601 (2007), p. 4733-41.

Mkrtchyan, M.M., Liddle, J.A., Berger, S.D., Harriott, L.R., Trajectory displacement effect in particle projection lithography systems: Modifications to the extended two-particle theory and Monte Carlo simulation technique, J. Appl. Phys. 78, (1995), p. 6888.

E. Munro, J. Rouse, H. Liu, and L. Wang, Aberration analysis of electron mirrors by a differential algebraic method. Optik, 2008, Vo. 119, No. 2, pp. 90-96.

D. Preikszas and H. Rose, J. Electron Microsc. 1, 1 (1997).

Schmidt, Th., H. Marchetto, P. L. Le´vesque, U. Groh, F. Maier, D. Preikszas, P. Hartel, R. Spehr, G. Lilienkamp, W. Engel, R. Fink, E. Bauer, H. Rose, E. Umbach, and H.-J. Freund, Ultramicroscopy 110, 1358 (2010).

Siwick, B.J., Dwyer, J.R., Jordan, R.E., Miller, R.J.D., Space charge effects in ultrafast electron diffraction and imaging, J. Appl. Phys. 92 (2002), p. 1643.

Tokita, S., M. Hashida, S. Inoue, T. Nishoji, K. Otani, and S. Sakabe, Electron diffraction using ultrafast electron bunches from a laser-wakefield accelerator at kHz repetition rate, Phys. Rev. Lett. 105 (2010) p. 215004.

Tromp, R. M., J.B. Hannon, A. W. Ellis, W. Wan, A. Berghaus, and O. Schaff, Ultramicroscopy 110, 852 (2010).

van Oudheusden, T., de Jong, E. F. , van der Geer, S. B. , Op 't Root, W. P. E. M., Luiten, O. J., Electron source concept for single-shot sub-100 fs electron diffraction in the 100 keV range, J. Appl. Phys. 102 (2007), p. 093501; doi: 10.1063/1.2801027

Wang, Y. and Gedik, N.,Electron Pulse Compression With a Practical Reflectron Design for Ultrafast Electron Diffraction, IEEE Journal of selected topics in quantum electronics, vol. 18, (2012), p. 140.